Interface solid-state reactions in LSM/SDC and LSM/BCY disclosed by X-ray microspectroscopy

Francesco Giannici,[1,*] Alessandro Chiara,[1] Giovanna Canu,[2,*] Alessandro Longo,[3,4] Antonino Martorana[1]

[1] Dipartimento di Fisica e Chimica, Università di Palermo, Viale delle Scienze, I-90128 Palermo, Italy

[2] Institute of Condensed Matter Chemistry and Technologies for Energy (CNR-ICMATE), Consiglio Nazionale delle Ricerche, via De Marini 6, I-16149 Genova, Italy

[3] Istituto per lo Studio dei Materiali Nanostrutturati (CNR-ISMN), Consiglio Nazionale delle Ricerche, via La Malfa 153, I-90146 Palermo, Italy

[4] Dutch-Belgian Beamline (DUBBLE), ESRF – The European Synchrotron, CS40220, F-38043 Grenoble, France

* corresponding authors: francesco.giannici@unipa.it; giovanna.canu@ge.icmate.cnr.it

Abstract

The stability of the electrode/electrolyte interface is a critical issue in solid-oxide cells working at high temperatures, affecting their durability. In this paper, we investigate the solid-state chemical mechanisms that occur at the interface between two electrolytes ($Ce_{0.8}Sm_{0.2}O_2$ – SDC, and $BaCe_{0.9}Y_{0.1}O_3$ – BCY) and a cathode material ($La_{0.8}Sr_{0.2}MnO_3$ – LSM) after prolonged thermal treatments. Following our previous work on the subject, we used X-ray microspectroscopy, a technique that probes the interface with submicrometric resolution combining microanalytical

information with the chemical and structural information coming from space-resolved X-ray absorption spectroscopy.

In LSM/BCY, the concentration profiles show striking reactive phenomena at the interface, with a variety of micrometer-sized secondary phases: in particular, X-ray absorption spectra reveal at least three different chemical states for manganese (from +3 to +6). Also in LSM/SDC, a couple previously reported as chemically stable, we found the formation of small islets of $SmMnO_3$ after the migration of manganese to the SDC side: these may constitute the nuclei for the subsequent formation of an interfacial resistive layer after more prolonged operation. The ability of manganese to adopt several oxidation states and crystal chemical environments is indicated as a possible cause for these behaviors.

Introduction

In the last decades, an ever increasing global interest towards the mitigation of environmental pollution has boosted the research on materials for renewable energy sources. Solid oxide fuel cells (SOFC), which convert chemical energy in electrical power without releasing waste products, play a relevant role in the sought-after integrated system of clean energy production: however, a number of materials science issues, involving reliability and durability of devices, are still under inspection.[1,2]

Prolonged operation of conventional SOFC systems at high temperature (around 900-1000 °C) can eventually lead to unwanted reaction between the various cell components. As an example, it is well known that yttria-stabilized zirconia (YSZ), one of the most common electrolyte materials for SOFC, reacts with strontium-containing electrodes to form the insulating secondary phase $SrZrO_3$.[3] The chemical compatibility between electrolytes and electrode materials is one of the most discussed issues to overcome in order to improve SOFC stability and to increase the life-time of the device. In particular, the study of solid-state reactivity between various SOFC components (interconnects, cermets, electrodes, etc.) is a forefront topic in materials research.[4-7] Different

approaches have been proposed to address such problems: e.g. interposing layers that impede the interdiffusion of cations and therefore prevent the formation of secondary phases,[8,9] or alternatively, developing materials that are able to perform well at lower temperatures. In recent years, the materials chemistry research in the field has been oriented towards the development of intermediate temperature SOFC (IT-SOFC), operating at about 600-700 °C.[10,11] We recently investigated the compatibility between two important materials for IT-SOFC: the cathode $La_{0.6}Sr_{0.4}Co_{0.2}Fe_{0.8}$ (LSCF) and the electrolyte $Ce_{0.8}Sm_{0.2}O_2$ (SDC).[12] In a LSCF/SDC bilayer treated at high temperature for prolonged time, we demonstrated for the first time that cation interdiffusion leads to the formation of a segregated $Sm(Co,Fe)O_3$ perovskite secondary phase. This led us to investigate other cathode/electrolyte couples for IT-SOFC.

LSM is a technologically relevant cathode for SOFC, and has been much studied for the last two decades, because of its high thermal and chemical stability, and good electronic conductivity.[13] However, the poor ionic conductivity at intermediate temperatures limits the application of $La_{1-x}Sr_xMnO_3$ as a suitable cathode for IT-SOFC devices. A way to overcome this drawback has been considered the formulation of composites made of $La_{1-x}Sr_xMnO_3$ and an electrolytic material such as YSZ or rare-earth-doped cerium oxide.[14-17]

Therefore, the stability under operation between electrolytic materials and LSM, either at a sharp interface or mixed together in a composite, is of the utmost relevance to determine the overall performance and durability of the cell. As a case study, we propose in this paper a detailed analysis of the microscopic compatibility between LSM and SDC, focussing on the diffusion processes and chemical state of the cations. SDC is one of the most used and investigated electrolytes for IT-SOFC, because of its appealing anionic conduction and chemical stability.[18,19] Aiming at obtaining further evidence of the solid state reactivity of LSM, we investigated also the interface LSM/BCY. BCY is a common electrolyte with protonic conduction and the couple LSM/BCY has deserved attention because of its encouraging performance.[20,21] As what concerns the compatibility between materials, both the LSM/SDC and LSM/BCY couples have been investigated in the past.[22,23] The

materials compatibility in SOFC devices is usually studied with bulk (e.g. XRD), or microanalytical techniques (e.g. SEM, SIMS, XPS microscopy). In this paper we used X-ray microspectroscopy, that combines the chemical and structural information about the environment of the different atomic species involved using micro-X-ray absorption near-edge structure (microXANES), with the advantages of an X-ray microprobe that provides spatially resolved maps of the investigated materials: we have successfully applied this approach recently, to evaluate materials compatibility in SOFC.[7,12]

We performed high-temperature annealing of the samples for 12-72 hours in order to simulate the thermal stress due to fabrication processes and operation. While LSM/SDC is commonly thought as a stable couple, presenting a fair structural compatibility, we nevertheless found a significant formation of $SmMnO_3$ islets at the interface, due to the migration of manganese. These may eventually grow to form a proper interface layer after prolonged operation. The LSM/BCY couple showed even more remarkable interface reaction, with a complex growth of three secondary phases organized in three layers: this most likely has a negative effect on the long-term performance of the cell.

Synthesis and characterization

Powders of $Ce_{0.8}Sm_{0.2}O_{2-x}$ (SDC) and $BaCe_{0.9}Y_{0.1}O_{3-x}$ (BCY) were prepared by solution combustion synthesis, using $Ce(NO_3)_3 \cdot 6H_2O$, $Sm(NO_3)_3 \cdot 6H_2O$, $Y(NO_3)_3 \cdot 6H_2O$ and $Ba(NO_3)_2$ (Sigma-Aldrich) as cation precursors. The details of the synthesis are reported elsewhere.[12] Phase purity of the electrolyte powders was verified by X-ray diffraction. $La_{0.8}Sr_{0.2}MnO_{3-x}$ (LSM) (Sigma-Aldrich) powder was used as received. The SDC and BCY powders were isostatically pressed (1500 bar) and sintered at 1550 °C for 4 hours, obtaining cylindrical samples with relative density of 96% for SDC and 90% for BCY. After cutting and polishing, pellets of about 10 mm diameter and 1 mm thickness were obtained: these were surrounded by LSM powder and uniaxially pressed at 7 tons in 1-inch die. The resulting bilayers were annealed in air at 1150 °C for either 12 or 72 hours, then

embedded in resin and cut to expose the interface. The samples were eventually polished down to 1 μm.

Scanning X-ray microscopy measurements with synchrotron radiation were carried out at the SXM-II end station of the ID21 beamline of ESRF (Grenoble, France).[24] The incident beam, was monochromatized with a double crystal Si monochromator and focused with Kirkpatrick-Baez mirrors. The samples were mounted with the interface parallel to the horizontal plane, and the sample stage was scanned in 2 dimensions with piezoelectric motors with respect to the fixed X-ray beam to acquire microXRF maps.

All microXRF and microXAS spectra were collected in fluorescence mode using a SDD detector at the Ce L_3-edge (5.72 keV) or the Mn K-edge (6.54 keV). At the Ce L_3-edge, the beam size was 450 x 450 nm^2 (H x V) with a flux of 10^{10} ph/s; at the Mn K-edge, the beam was 450 x 750 nm^2 (H x V) with a flux of $7 \cdot 10^{10}$ ph/s. Data reduction and analysis was performed with PyMca.[25] The data were corrected for the incident beam intensity and for detector dead-time, and analyzed using a self-consistent XRF fitting to take into account self-absorption and matrix effects.

Result and discussion

The samples were treated at high temperature for either 12 or 72 h, in order to simulate the SOFC fabrication temperature and operation. X-ray fluorescence (XRF) was employed to investigate the interdiffusion of cations after annealing. Starting from the elemental maps, the distance/concentration profiles are calculated perpendicularly to the electrode/electrolyte interface and horizontally averaged over tens of microns. We then used micro-X-ray absorption near edge structure (microXANES) spectra at Mn or Ce absorption edges in selected spots to obtain information about the oxidation state and the chemical environment of the cations.

LSM/SDC

In LSM/SDC annealed for 12 hours the diffusion profiles are rather sharp (see Figure 1), except for manganese and samarium that present a some diffusion (around 5 μm). The manganese profile, far in the bulk of LSM, shows a peculiar shape due to accumulation spots of manganese visible in the fluorescence map.

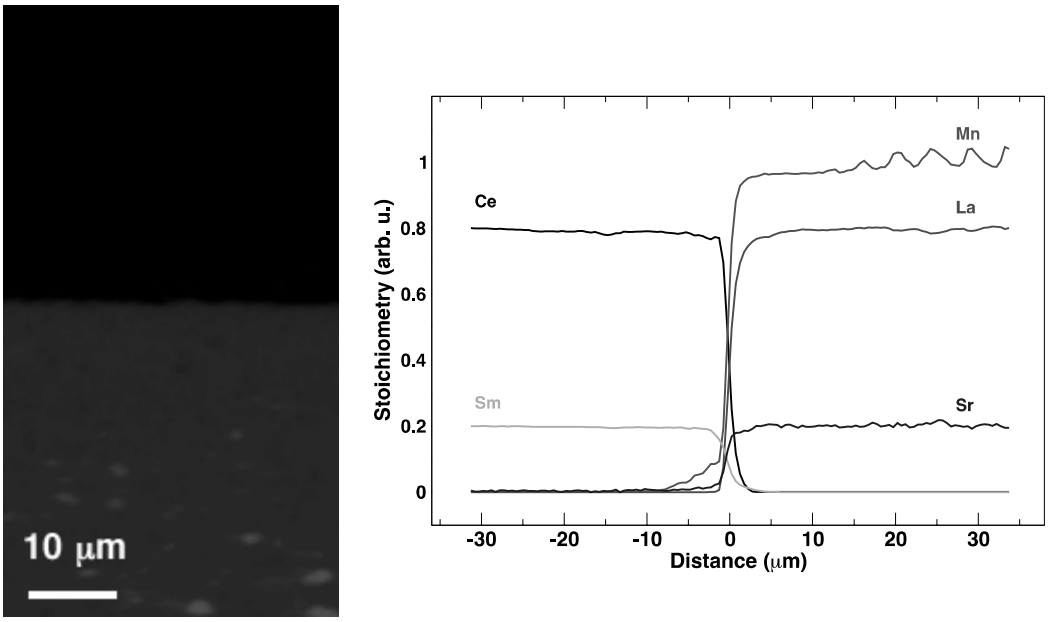

Figure 1 – LSM/SDC 12h at the Mn K-edge. Left: concentration map of manganese (red); right: concentration profiles of cerium (black), lanthanum (red), strontium (blue), samarium (orange), and manganese (green).

In LSM/SDC annealed for 72 hours (see Figure 2), samarium diffuses for about 5 μm, and its diffusion seems to be correlated with a decrease of lanthanum. Owing to its fairly large ionic radius, the insertion of samarium in the perovskite A-site does not change much its tolerance factor.[26] Compared to the case of LSM/SDC annealed for 12 hours, the accumulation spots of manganese in the bulk region of LSM are not observed (Figure 2 and 3). This can be explained by an enhanced diffusion of manganese after 72 hours which helps smoothening the accumulation spots. In the SDC region, a correlation can be observed between samarium, manganese and cerium. In particular, the Mn segregation occurs together with Sm, at the expense of Ce.

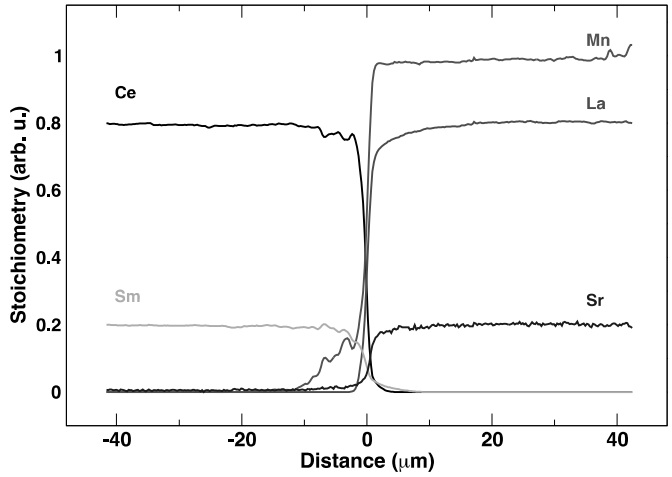

Figure 2 – LSM/SDC 72h at the Mn K-edge. Concentration profiles of cerium (black), lanthanum (red), strontium (blue), samarium (orange), and manganese (green).

This behavior is even more evident by inspecting the elemental maps in Figure 3, where localized accumulation of Sm and Mn is evident near the interface in the SDC region, corresponding to a depletion of Ce. We did observe a similar effect in the electrolyte/electrode couple LSCF/SDC,[12] with a similar correlation between iron, samarium and cerium. Also in LSM/SDC there is an important segregation of manganese and samarium in the SDC region, forming perovskite islands of $SmMnO_3$ about 1-2 μm in size. The formation of $SmMnO_3$ will further substantiated when discussing the microXANES results.

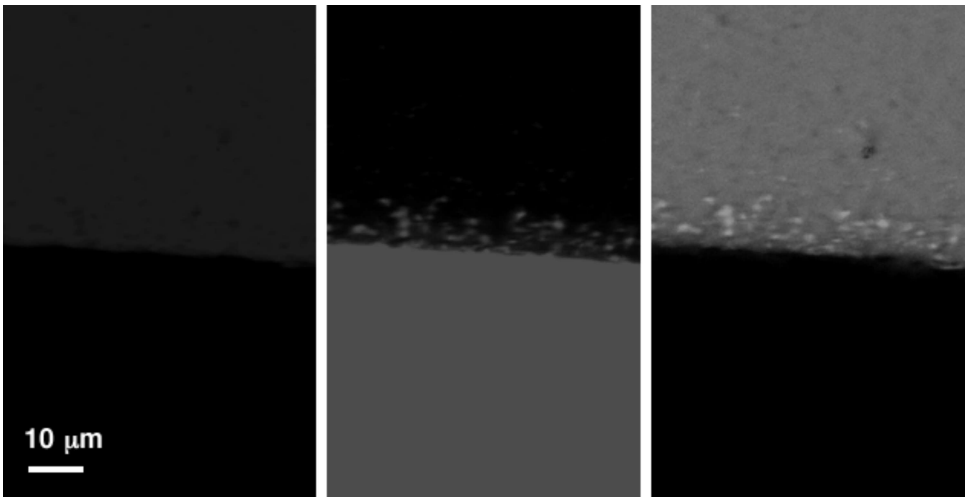

Figure 3 – LSM/SDC 72h at the Mn K-edge. Left to right: concentration maps of cerium (blue), manganese (red) and samarium (green).

Ce L_3-edge microXANES spectra measured in spots 1 to 10 (see Figure 4) display a broad variability, which reflects the different chemical and structural environments of the cerium cations between SDC and LSM regions. Starting with spot 1 (in bulk SDC), the spectrum is typical of Ce^{4+} in a fluorite structure. When diffusing into LSM, the XANES white line increases in intensity and shifts to lower energies: both effects are typical of a reduction from Ce^{4+} to Ce^{3+}. It is likely that Ce^{3+}, when incorporated into the LSM structure, is able to replace La^{3+} in the A-site of the perovskite, as their ionic radii are quite similar (1.34 Å for Ce^{3+} vs. 1.36 Å for La^{3+}).[27]

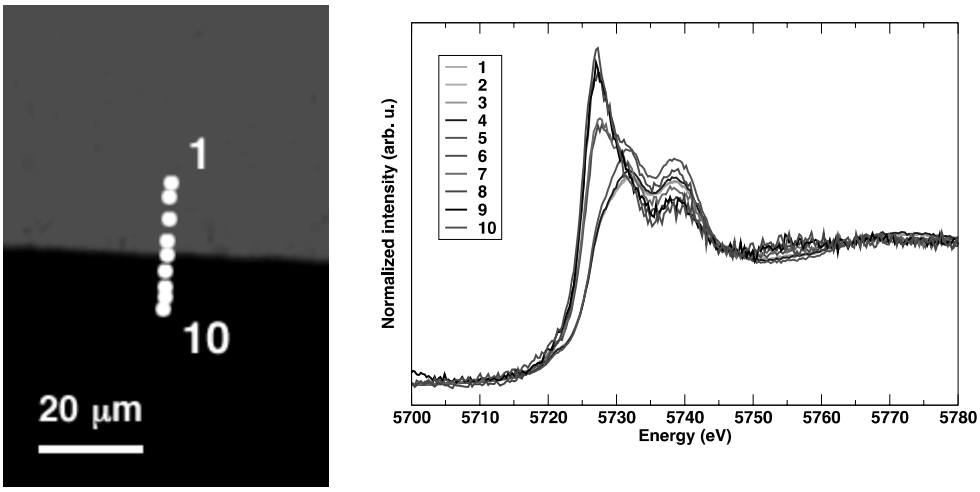

Figure 4 – LSM/SDC 72h at the Ce L_3-edge. Left: concentration map of cerium (red). Right: Ce L_3-edge microXANES spectra measured at different points shown in the left panel.

At the Mn K-edge the overall shape of the microXANES spectra (reported in Figure 5) is unchanged in the different spots examined in both the SDC and LSM regions: this means that manganese preserves the perovskite environment with octahedral coordination while diffusing through the interface. On the other hand, it is known that the oxidation state of Mn in LSM (between +3 and +4) is affected by the presence in the A-site of bivalent and trivalent species, combined with other charge-balance mechanisms.[28,29] Actually, at a closer inspection, when Mn diffuses in the SDC region (spots 1 to 7), the microXANES spectra shift slightly to the left, with an increase of the edge shoulder at 6548 eV, meaning that the oxidation state of Mn is lowered. Since the overall shape of the spectrum is maintained, while the oxidation state is lowered, it can be safely concluded that manganese segregates into perovskite islands of $SmMnO_3$, with a Mn^{3+} oxidation state.

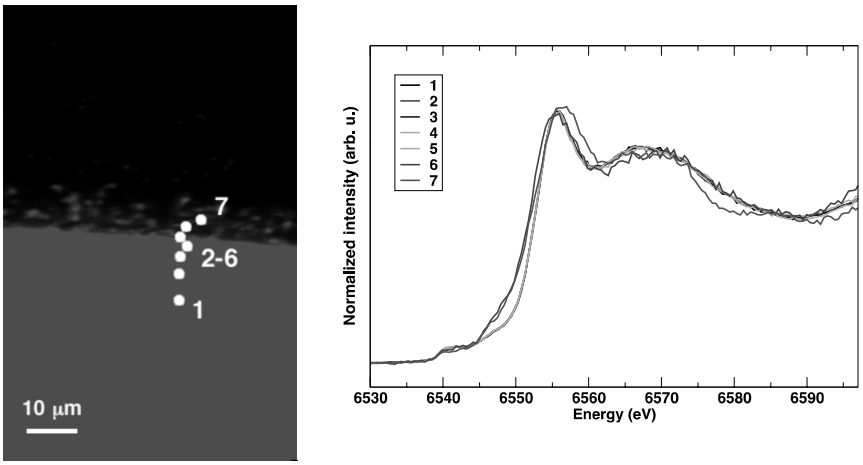

Figure 5 – LSM/SDC 72h at the Mn K-edge. Left: concentration map of manganese (red). Right: Mn K-edge microXANES spectra measured at different points shown in the left panel.

LSM/BCY

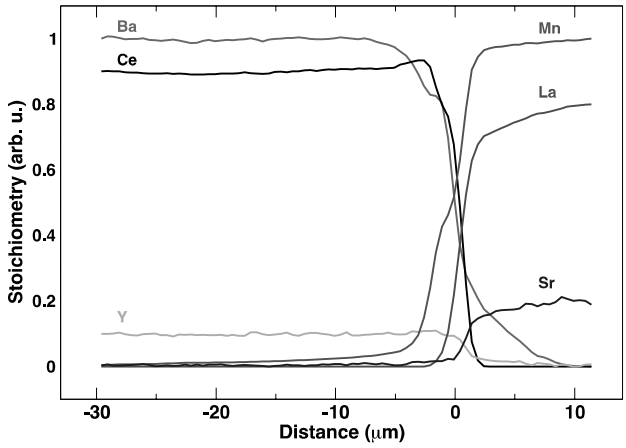

Figure 6 – LSM/BCY 12h at the Mn K-edge. Concentration profiles of barium (pink), cerium (black), yttrium (orange), manganese (green), lanthanum (red) and strontium (blue).

In LSM/BCY the interdiffusion between electrolyte and cathode is already evident after 12 hours of annealing (see Figure 6). The diffusion of barium (around 10 μm) in LSM is accompanied by a counterdiffusion of lanthanum and strontium. It is well know that barium can replace lanthanum in the A-site of the perovskite LSM.[30] Cerium shows a slight enrichment in BCY close to the interface (around 2 μm). In the same region of BCY, the barium profile shows a shoulder. Manganese diffuses in a considerable amount for about 3 μm, then it is found as far as 18 μm beyond the interface in smaller amount. The shoulder in the diffusion profile of manganese occurs at the same depth as a similarly shaped feature in the profile of barium.

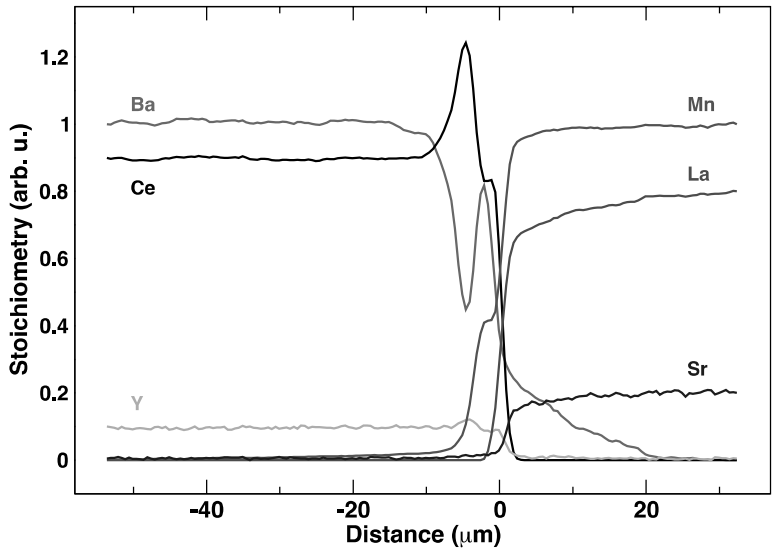

Figure 7 - LSM/BCY 72h at the Mn K-edge. Concentration profiles of barium (pink), cerium (black), yttrium (orange), manganese (green), lanthanum (red) and strontium (blue).

In LSM/BCY annealed for 72 hours (see Figure 7), the reaction between the electrolyte and the cathode materials is even more extensive, with several interesting structures in the interface region. Starting from the LSM side, a significant enrichment of barium is found as far as 20 μm. Then, in the interface region, it is possible to recognize three secondary phases, marked by sharp features visible both in the profiles and in the elemental maps: first, a Ce and Y-rich phase (at 0 μm); next, a Ba and Mn-rich phase (at -1 μm); lastly, a depletion of Ba and increase of Ce gives rise to a further Ce and Y-rich phase (at -5 μm).

The sequence of these layering phases can be best understood going from bottom to top in the elemental maps of Figure 8.

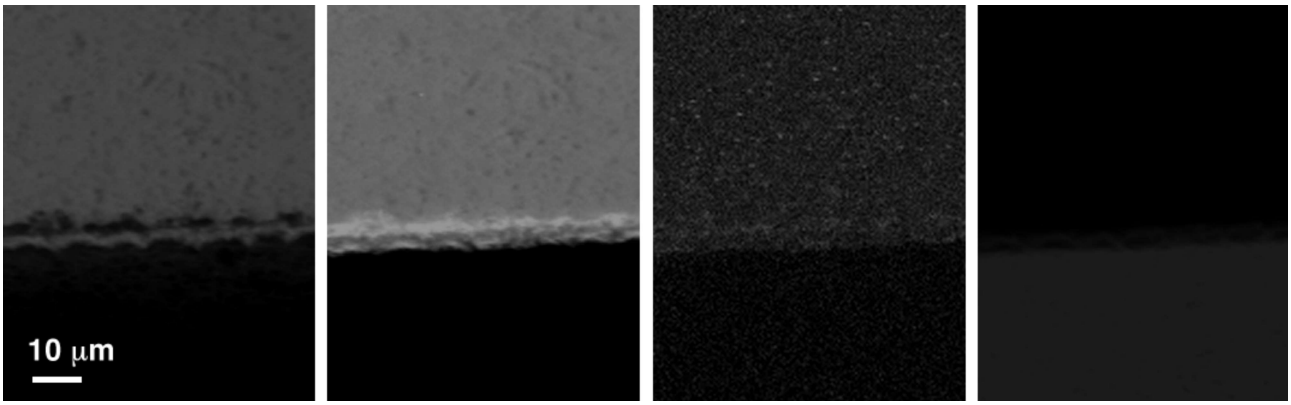

Figure 8 - LSM/BCY 72h at the Mn K-edge. Left to right: concentration maps of barium (red), cerium (green), yttrium (violet), manganese (blue).

The Ba- and Mn-rich layer has a peculiar shape, with small arcs 7-10 μm wide, where the bottom part of the arc touches the LSM region (see Figure 8). Both above and below this layer, the presence of a Ce- and Y-rich phase is highlighted by the superposition of the maps of barium (red) and cerium (green) (Figure 9, left), while the Ba-Mn arcs are evidenced by the superposition of barium (red) and manganese (green) (Figure 9, right). The depletion of barium and manganese in the outer interface layers is clear.

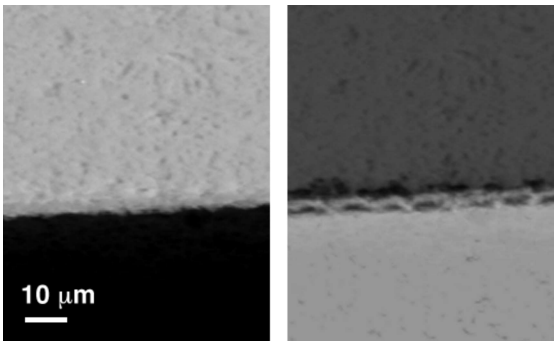

Figure 9 - LSM/BCY 72h at the Mn K-edge. Left: concentration map of barium (red) and cerium (green); the superposition of the two elements appears as orange. Right: concentration map of barium (red) and manganese (green).

Looking at Ce L_3-edge microXANES (Figure 10) of LSM/BCY it is possible to identify three different chemical environments for cerium: 1) octahedrally coordinated Ce^{4+} in the BCY bulk;[31] 2) Ce^{4+} in doped ceria, as it is evident by the position and height of the double edge features;[32] 3) a partially reduced Ce^{4+}/Ce^{3+} state in the LSM region, as witnessed by the shift to lower energies of the edge structures. As it is the case for the LSM/SDC couple, it seems likely that Ce^{3+} can be stabilized in the A-site of the perovskite structure, substituting lanthanum. CeO_2 had already been detected as one of the products of the solid state reaction between BCY and LSM.[23]

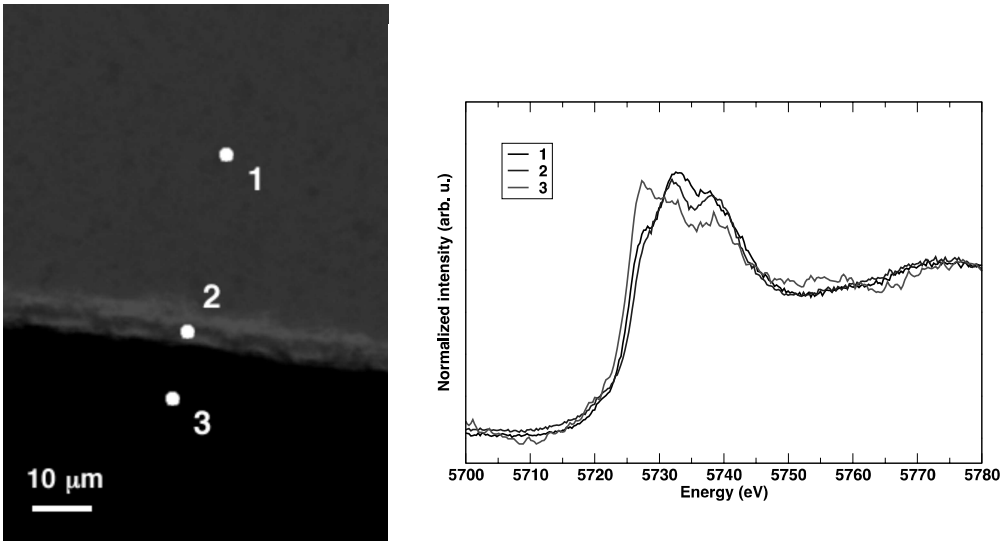

Figure 10 – LSM/BCY 72h at the Ce L_3-edge. Left: concentration map of cerium with the spots where microXANES spectra were recorded. Right: Ce L_3-edge microXANES spectra.

At the Mn K-edge (Figure 11), the microXANES spectra show striking variations across the interface. The representative spectra show the modification of oxidation state and chemical environment of manganese. In particular: 1) in bulk LSM, $Mn^{3+\delta}$ is placed in an octahedral coordination; 2) moving to the interface, the edge features closely resemble those of $BaMnO_3$,[33] coherently with the Ba-enrichment found at the interface: the edge shift towards higher energy confirms the presence of Mn^{4+}; 3) in the BCY region, the spectrum features a prominent pre-edge around 6541 eV, which is indicative of tetrahedrally coordinated Mn^{6+} in a $BaMnO_4$ structure.[34]

Lygaeva et al. reported the presence of YMn_2O_5 as a secondary phase in the mixture of BCY and LSM powders after annealing.[23] However, none of the spectra of Figure 11 shows resemblance with the near-edge features of YMn_2O_5.[35]

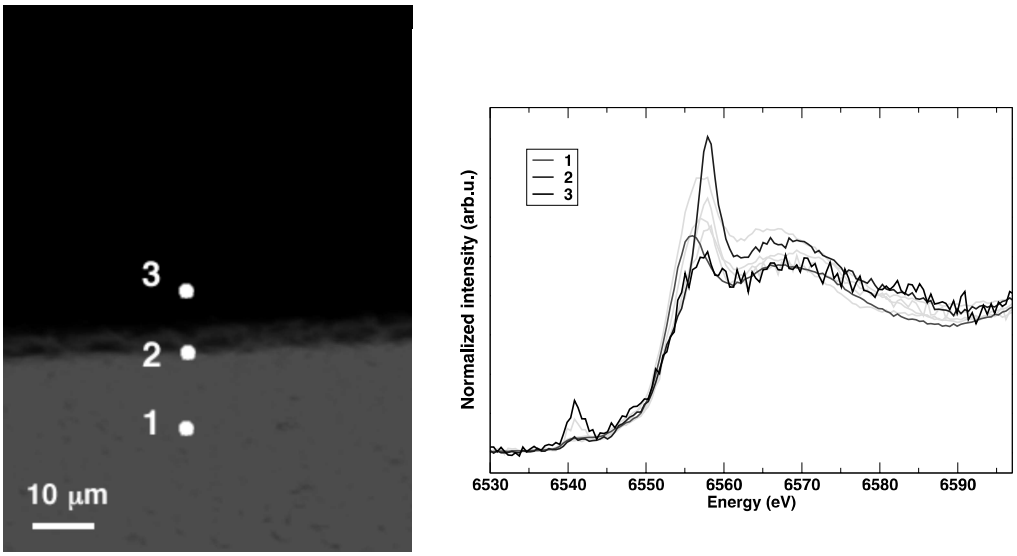

Figure 11 - LSM/BCY 72h at the Mn K-edge. Left: Concentration map of manganese (red). Right: Mn K-edge microXANES spectra in spots 1-3 (black, red and blue); spectra acquired between spots 1 to 3 are plotted in grey to underline the continuous changes in the spectra.

As a final remark, it can be observed that in both LSM/BCY and LSM/SDC the diffusivity and solid state reactivity of manganese seems to play an important role in the interface structure of these cathode/electrolyte couples. SIMS analysis performed on a LSM microcathode deposited on YSZ and SPEM (Scanning PhotoElectron Microscopy) on a LSM/YSZ performed under polarization conditions demonstrated also for these electrolyte/electrode couples the role of Mn diffusion in determining the electrochemical properties of the assembly.[36,37] In particular, Backhaus-Ricoult et al. associated the diffusion of reduced Mn into the electrolyte under cathodic bias with the enhancement of the electrochemical activation of the cathode.[37] The present results demonstrate that the diffusion of Mn plays an important role in the stability of the electrolyte/cathode couple, also in the absence of an electrical polarization, and also in the bulk electrolyte region. In particular, it

seems that the ability of Mn to adopt a wide range of oxidation states and its versatility in forming different compounds with Ba, La and Sm, all may affect the long-term stability and the operation of the device.

Conclusions

X-ray microspectroscopy has demonstrated to be a powerful technique for the study of electrolyte/electrode couple stability. Here we studied the stability between LSM, one of the most widespread cathodic materials for IT-SOFC, with two representative electrolytes: SDC and BCY. The interaction between SDC and LSM causes a general interdiffusion of cations across the interface: moreover, the formation of small spots of manganese and samarium inside the SDC region is observed. MicroXANES spectra show that even if manganese diffuses across the interface, its octahedral coordination is retained: in fact, the formed islets show a perovskite $SmMnO_3$ structure. Cerium after diffusion across the interface is incorporated in the A-site of the LSM perovskite, changing its oxidation state from Ce^{4+} to Ce^{3+}.

In the BCY/LSM couple, due to significant interdiffusion of cations, the formation of three interface layers can be observed. The central phase is characterized by an enhanced Ba-Mn composition of barium and manganese, identified as a $BaMnO_3$ perovskite. Around this phase, two other secondary growths are evident in the elemental XRF maps: these are much enriched in Ce and Y, and correspondingly depleted in Ba and Mn, suggesting the formation of Y-doped ceria.

The microXANES spectra are used to corroborate these proposed compositions, showing three different chemical environments for cerium: 1) Ce^{4+} in BCY, 2) Ce^{4+} in doped ceria, in the interface region -10-0 μm, 3) Ce^{3+} incorporated in LSM. The microXANES spectra on Mn K-edge show three different chemical environments too: 1) $Mn^{3+\delta}$ in LSM, 2) Mn^{4+} in the secondary phase with $BaMnO_3$ structure, 3) Mn^{6+} in the BCY region, hinting to the formation of $BaMnO_4$.

Both electrolyte/cathode couples show an appreciable interdiffusion of cations at the present experimental conditions. The results of this work highlights the overall poor chemical and structural

stability of the LSM/BCY couple, because of the formation of three different secondary phases at the interface, that probably influence negatively the cell performance. The LSM/SDC couple shows a better chemical stability, but the formation of an archipelago of $SmMnO_3$ islets seems to prelude, also in this case, to the growth of a secondary layered phase at the electrolyte/electrode interface.

In both LSM/SDC and LSM/BCY interfaces, Mn diffusivity and solid state reactivity seem to play a crucial role in the formation of interface secondary phases: while a previous study suggested that this effect happened in conjunction to an electrical polarization on the surface, in this paper we confirm that this is not limited to the surface, and may also happen in absence of an external electrical field. The wide variety of chemical states which Mn is able to adopt favors its inclusion in secondary growths which may affect the long-term operation.

Acknowlegdements

We acknowledge funding through MIUR projects Futuro in Ricerca "INnovative Ceramic and hYbrid materials for proton conducting fuel cells at Intermediate Temperature: design, characterization and device assembly (INCYPIT)", PON R&C "Tecnologie ad alta Efficienza per la Sostenibilità Energetica ed ambientale On-board (TESEO)", PRIN "Celle a combustibile ad ossido solido operanti a temperatura intermedia alimentate con biocombustibili (BIOITSOFC)". We acknowledge the ESRF for provision of beamtime, and we thank the staff of beamline ID21 for assistance during the measurements. We thank Dr. Wout De Nolf (ESRF) for useful discussions and assistance during data analysis.

(1) Yokokawa, H.; Tu, H.; Iwanschitz, B.; Mai, A. Fundamental mechanisms limiting solid oxide fuel cell durability. *J. Power Sources* **2008**, 182, 400-412.

(2) Yokokawa, H. Understanding materials compatibility. *Annu. Rev. Mater. Res.* **2003**, 33, 581-610.

(3) Tu, H. Y.; Takeda, Y.; Imanishi, N.; Yamamoto, O. $Ln_{0.4}Sr_{0.6}Co_{0.8}Fe_{0.2}O_{3-\delta}$ (Ln=La, Pr, Nd, Sm, Gd) for the electrode in solid oxide fuel cells. *Solid State Ionics* **1999**, 117, 277-281.

(4) Liu, Y. L; Chengge J. Microstructure degradation of an anode/electrolyte interface in SOFC studied by transmission electron microscopy. *Solid State Ionics* **2005**, 176, 435-442.

(5) Matsui T.; Mikami, Y.; Muroyama, H.; Eguchi, K. Influence of $(La,Sr)MnO_{3-\delta}$ cathode composition on cathode/electrolyte interfacial structure during long-term operation of solid oxide fuel cells. *J. Power Sources* **2013**, 242, 790-796.

(6) Matsui, T.; Komoto, M.; Muroyama, H.; Eguchi, K. Interfacial Stability between Air Electrode and Ceria-Based Electrolyte under Cathodic Polarization in Solid Oxide Fuel Cells. *Fuel Cells* **2014**, 14, 1022-1027.

(7) Giannici, F.; Canu, G. Gambino, M.; Longo, A.; Salomé, M.; Viviani, M.; Martorana, A. Electrode–Electrolyte Compatibility in Solid-Oxide Fuel Cells: Investigation of the LSM–LNC Interface with X-ray Microspectroscopy. *Chem. Mater.* **2015**, 27, 2763-2766.

(8) Matsuda, M.; Hosomi, T.; Murata, K.; Fukui, T; Miyake, M. Fabrication of bilayered YSZ/SDC electrolyte film by electrophoretic deposition for reduced-temperature operating anode-supported SOFC. *J. Power Sources* **2007**, 165, 102-107.

(9) Nguyen, H. V. P.; Hardy, J. S.; Coyle, C. A.; Lu, Z.; Stevenson, J. W. Developing Cost-Effective Dense Continuous SDC Barrier Layers for SOFCs. *ECS Transactions* **2017**, 75, 107-114.

(10) Sinha, A.; Miller, D.N.; Irvine, J.T.S. Development of novel anode material for intermediate temperature SOFC (IT-SOFC). *J. Mater.Chem. A* **2016**, 4, 11117–11123.

(11) Fan, X.; You, C.; Zhu, J.; Chen, L.; Xia, C. Fabrication of LSM-SDC composite cathodes for intermediate-temperature solid oxide fuel cells. *Ionics* **2015**, 21, 2253–2258.

(12) Giannici, F.; Canu, G.; Chiara, A.; Gambino, M.; Aliotta, C.; Longo, A.; Buscaglia, V.; Martorana, A. Cation diffusion and segregation at the interface between samarium-doped ceria and LSCF or LSFCu cathodes investigated with X-ray microspectroscopy. *ACS Appl. Mater. Interfaces* **2017**, 9, 44466-44477.

(13) Skinner, S. J. Recent advances in Perovskite-type materials for solid oxide fuel cell cathodes. *Int. J. Inorg. Mater.* **2001**, 3, 113-121.

(14) Jørgensen, M. J.; Mogensen, M. Impedance of solid oxide fuel cell LSM/YSZ composite cathodes. *J. Electrochem. Soc.* **2001**, 148, A433-A442.

(15) Murray, E. P.; Barnett, S. A. (La, Sr)MnO_3–(Ce, Gd)O_{2-x} composite cathodes for solid oxide fuel cells. *Solid State Ionics* **2001**, 143, 265-273.

(16) Xu, X.; Jiang, Z.; Fan, X. LSM–SDC electrodes fabricated with an ion-impregnating process for SOFCs with doped ceria electrolytes. *Solid State Ionics* **2006**, 177, 2113-2117.

(17) Navarrete, L.; Balaguer, M.; Vert, V. B.; Serra J. M. Optimization of SOFC Composite Cathodes Based on LSM and Doped Cerias $Ce_{0.8}Ln_{0.2}O_{2-\delta}$ (Ln = Gd, Er, Tb and Pr). *J. Electrochem. Soc.* **2016**, 163, F1440-F1443.

(18) Steele, B.C.H. Appraisal of $Ce_{1-y}Gd_yO_{2-y/2}$ electrolytes for IT-SOFC operation at 500°C. *Solid State Ionics* **2000**, 129, 95.

(19) Kharton, V.V.; Marques, F.M.B.; Atkinson, A. Transport properties of solid oxide electrolyte ceramics: a brief review. *Solid State Ionics* **2004**, 174, 135.

(20) Lee, K.; Choi, M.; Lim, D.; Singh, B.; Song, S. Effect of humidification on the performance of intermediate-temperature proton conducting ceramic fuel cells with ceramic composite cathodes. *J. Power Sources* **2013**, 232, 224-233.

(21) Lim, D.; Im, H.; Singh, B.; Song, S. Investigations on electrochemical performance of a proton-conducting ceramic-electrolyte fuel cell with $La_{0.8}Sr_{0.2}MnO_3$ cathode. *J. Electrochem. Soc.* **2015**, 162, F547-F554.

(22) Jin, C.; Liu, J.; Guo, W.; Zhang, Y. Electrochemical characteristics of an $La_{0.6}Sr_{0.4}Co_{0.2}Fe_{0.8}O_3$–$La_{0.8}Sr_{0.2}MnO_3$ multi-layer composite cathode for intermediate-temperature solid oxide fuel cells. *J. Power Sources* **2008**, 183, 506-511.

(23) Lyagaeva, J.; Medvedev, D.; Pikalova, E.; Plaksi, S.; Brouzgou, A.; Demin, A.; Tsiakaras, P. A detailed analysis of thermal and chemical compatibility of cathode materials suitable for

$BaCe_{0.8}Y_{0.2}O_{3-\delta}$ and $BaZr_{0.8}Y_{0.2}O_{3-\delta}$ proton electrolytes for solid oxide fuel cell application. *Int. J. Hydrog. Energy* **2017**, 42, 1715-1723.

(24) Salome, M.; Cotte, M.; Baker, R.; Barrett, R.; Benseny-Cases, N.; Berruyer, G.; Bugnazet, D.; Castillo-Michel, H.; Cornu, C.; Fayard, B.; Gagliardini, E.; Hino, R.; Morse, J.; Papillon, E.; Pouyet, E.; Rivard, C.; Sole, V. A.; Susini, J.; Veronesi, G. The ID21 Scanning X-ray Microscope at ESRF. *J. Phys. Conf. Series* **2013**, 425, 182004.

(25) Solé, V. A.; Papillon, E.; Cotte, M.; Walter, P.; Susini, J. A. multiplatform code for the analysis of energy-dispersive X-ray fluorescence spectra. *Spectrochim. Acta B* **2007**, 62, 63-68.

(26) Chourasia R.; Shrivastava O. P. Crystal structure and impedance study of samarium substituted perovskite: $La_{1-x}Sm_xMnO_3$ (x= 0.1–0.3). *Solid State Sci.* **2012**, 14, 341-348

(27) Oliva, C.; Allieta, M.; Scavini, M.; Biffi, C.; Rossetti, I.; Forni, L. Electron Paramagnetic Resonance Analysis of $La_{1-x}M_xMnO_{3+\delta}$ (M=Ce, Sr) Perovskite-Like Nanostructured Catalysts. *Inorg. Chem.* **2012**, 51, 8433-8440.

(28) Abbate, M.; de Groot, F. M. F.; Fuggle, J. C.; Fujimori, A.; Strebel, O.; Lopez, F.; Domke, M.; Kaindl, G.; Sawatzky, G.A.; Takano, M.; Takeda, Y.; Eisaki, H.; Uchida, S. Controlled-valence properties of $La_{1-x}Sr_xFeO_3$ and $La_{1-x}Sr_xMnO_3$ studied by soft-x-ray absorption spectroscopy. *Physical Review B* **1992**, 46, 4511-4519.

(29) Pandey, S. K.; Bindu, R.; Kumar, A.; Khalid, S.; Pimpale, A. V. Doping and bond length contributions to Mn K-edge shift in $La_{1-x}Sr_xMnO_3$ (x=0–0.7) and their correlation with electrical transport properties. *Pramana* **2008**, 70, 359-366.

(30) Dabrowski, B.; Rogacki, K.; Xiong, X.; Klamut, P. W.; Dybzinki, R.; Shaffer, J. Synthesis and properties of the vacancy-free $La_{1-x}Ba_xMnO_3$. *Physical Review B* **1998**, 58, 2716-2723.

(31) Seidel, S.; Patzig, C.; Krause, M.; Höche, T.; Gawronski, A.; Hu, Y.; Rüssel, C. The effect of CeO_2 on the crystallization of MgO-Al_2O_3-SiO_2-ZrO_2 glass. *Mater. Chem. Phys.* **2018**, 212, 60-68.

(32) Giannici, F.; Gregori, G.; Aliotta, C.; Longo, A.; Maier, J.; Martorana, A. Structure and Oxide Ion Conductivity: Local Order, Defect Interactions and Grain Boundary Effects in Acceptor-Doped Ceria. *Chem. Mater.* **2014**, 26, 5994-6006.

(33) Chaboy, J.; Prieto, C.; Hernando, M.; Parras, M.; González-Calbet, J. Ab initio X-ray absorption study of the manganese K-edge XANES spectra in Mn-and Zn-related hexagonal perovskites. *Phys. Rev. B* **2006**, 74, 174433.

(34) Muller-Bouvet, D.; Emery, N.; Tassali, N.; Panabiere, E.; Bach, S.; Crosnier, O.; Brousse, T.; Cenac-Morthe, C.; Michalowicz, A.; Pereira-Ramos, J.P. Unravelling redox processes of Li_7MnN_4 upon electrochemical Li extraction–insertion using operando XAS. *Phys. Chem. Chem. Phys.* **2017**, 19, 27204-27211.

(35) Wunderlich, F.; Leisegang, T.; Weissbach, T.; Zschornak, M.; Stöcker, H.; Dshemuchadse, J.; Lubk, A.; Führlich, T.; Welter, E.; Souptel, D.; Gemming, S.; Seifert, G.; Meyer, D. C. EXAFS, XANES, and DFT study of the mixed-valence compound YMn_2O_5: Site-selective substitution of Fe for Mn. *Phys. Rev. B* **2010**, 82, 014409.

(36) Hansen, K. V.; Norrman, K.; Jacobsen, T.; Wu, Y.; Mogensen, M. G. LSM Microelectrodes: Kinetics and Surface Composition. *J. Electrochem. Soc.* **2015**, 162, F1165-F1174.

(37) Backhaus-Ricoult, M.; Adib, K.; St.Clair, T.; Luerssen, B.; Gregoratti, L.; Barinov, A. In-situ study of operating SOFC LSM/YSZ cathodes under polarization by photoelectron microscopy. *Solid State Ionics* **2008**, 179, 891–895.